NON-CONVENTIONAL PET NUCLIDES: PRODUCTION AND IMAGING

NUCLEIDOS DE PET NO CONVENCIONALES: PRODUCCIÓN Y PROYECCIÓN DE IMAGEN

Richard Laforest

Washington University School of Medicine (Mallinckrodt Institute of Radiology, St.Louis, USA)

Abstract

Medical cyclotrons are now commonly used for the production of PET nuclides by the (pn) reaction. These devices are typically capable of delivering 10-15 MeV protons beams at sufficiently high intensity for timely production of β^+ decaying nuclides. Non-conventional PET nuclides have emerged recently and offers new opportunities for diagnostic and therapy drug discovery. In this paper, we will review the production capabilities for such nuclides at Washington University Medical School in St. Louis and present their production. Finally, challenges for imaging imposed by the specific of the decay characteristics will be discussed.

Resumen

Los ciclotrones médicos son usados actualmente para la producción de Nucleidos de PET. Esos dispositivos son capaces de producir haces de protones de 10-15 MeV con suficiente intensidad para la producción de radionúcleos con decaimiento β^+. Los nucleidos no convencionales de PET

Richard Laforest: laforestr@wustl.edu

han surgido recientemente y ofrecen nuevas oportunidades para diagnóstico y farmacoterapia. En este artículo se hará mención de la capacidad de producción de tales nucleidos en la Washington University Medical School. Serán discutidos los retos en imagenología impuestos por las características del decaimiento.

Palabras clave: Radionúcleos de PET, cascada de rayos gama, ciclotrón, rango de positrones.

Introduction

Radio-nuclides are widely used in medicine for imaging and radiotherapy applications. For imaging, β^+ decaying nuclides are of special interest since the simultaneous emission of acolinear annihilation photons can be exploited to detect the localization of the spatial position of the activity. Contrary to single photon emission imaging, where the localization of the emission point is permissible only through the use of collimators, which themselves yields to significant reduction of sensitivity and spatial resolution, the coincident detection of the positron annihilation photons in PET (Positron Emission Tomography), allows for electronic collimation. This so called electronic collimation is responsible for the high sensitivity of PET cameras and thus high collection speed. These reasons have led to the high interest in PET for radiopharmaceuticals development for imaging and therapy, and thus the motivation for the wide interest in using this technology is to determine the spatial and temporal localization of imaging agents within the living human body.

PET of course started with the development of cameras that were initially used exclusively for bio-medical research in large institutions. The technology being inherently expensive, due to the cost of the machine but also due to the necessity of nearby cyclotrons. The advent of ^{18}F-fluorodeoxyglucose (FDG), an ^{18}F labeled glucose analog, propelled the use of this technology in the routine clinical arena in the 1990s and made this technology part of the standard of care of thousands of medical institutions in the

world. The half-live of this nuclide (approximately 2hr) and the relatively low positron energy (average of 250 keV) are important factors that allowed the technology to grow. ^{18}F is a pure β^+ nuclide with a half-life ideal for radio-labeling, distribution and also in providing acceptable radiation dose to the patient.

FDG is an analog of glucose but unlike glucose, FDG is metabolized in a different way. FDG will be transported into the cells by the same mechanism as glucose but the labeling position of the ^{18}F nuclide will prevent complete metabolization and will yield to trapping of the activity within the cells. Cancerous cells, being particular demanding in energy, will thus predominantly accumulate activity. FDG has thus become an essential tool in the armamentarium for the diagnosis, staging and evaluation or therapy effectiveness for many forms of cancers. Other nuclides have played a role in the early development of PET, such as ^{11}C attached to a plethora of agents for various neuro-receptor studies, ^{15}O-Water for cerebral blood flow analysis and ^{13}NH3 cardiac perfusion and blood flow measurements. Those continue to be used intensively for PET imaging. These nuclides are now described as standard PET nuclides and are routinely produced with low energy medical cyclotrons. Some nuclides of common use can be produced by generators (e.g. ^{82}Rb, ^{62}Cu, ^{68}Ga).

However those are not the only nuclides used for PET, many other proton rich nuclides can be used and those are of special interest for the development of novel radio-pharmaceuticals for diagnostic and radio-therapy applications and are an important part of the research being conducted at Washington University School of Medicine in St. Louis (USA). These so-called non-standard or non-conventional PET nuclides will be the subject of this presentation.

This chapter will present the production capabilities of radio-nuclides, describing the technology and some applications, notably for the imaging of novel imaging pathways that can shed light on the tumor biology itself. The document will focus on

the presentation of the technology and will include a discussion of the imaging aspects with such nuclides. This chapter is the part of a three lectures series discussing the production of PET radio-nuclides. The second and third chapters will discuss the PET technology itself and the image reconstruction process while the last chapter will present the current status of the technology in research and clinical setting along with the current technical challenges and research opportunities being addressed.

Medical Isotopes from Cyclotrons

Medical cyclotrons consist typically of compact supra-conducting accelerating devices capable of producing proton and deuteron beams at approximately 15 MeV. Washington University School of Medicine in St.Louis currently operates 4 of these instruments. These include: the CS-15 (Cyclotron Corporation), JSW (Japan Steel Work), RDS-111 (Siemens), and the TR-19/9 (Advanced Cyclotron Systems). This one was installed over the summer of 2014 and will eventually replace the older CS-15 and JSW after their decommissioning. At 10-15 MeV, the most favorable method of production is from the production of excited compound nucleus by the (p,n), (p,α) or (d,n) reaction. The produced radio-nuclides remains essentially trapped in the target and need to be extracted by physical-chemistry methods.

Cu-64 Production

Cu-64 has tremendous interest at our institution and at many others in the world due to its favorable decay characteristics for PET imaging. The end point positron energy (identical to ^{18}F) makes it an ideal PET nuclide for high-resolution and also its half-life of 12.7 hr allows for imaging up to 48 hr post injection. It is currently used for imaging the biodistribution of molecules targeting tumors. The combined β^+ and β^- makes this nuclide also of interest for radiotherapy applications due to the potential of delivering targeted therapy radiation doses. This nuclide is produced by the (p,n) reaction of electroplated ^{64}Ni on a Au disk.

Nuclide	Half-Life	Decay-Mode/%	Max energy (MeV)	Target Material and natural abundance
^{76}Br[1, 2]	16.2 hr	β^+/57 EC/43	3.98	^{76}Se/9.1 %
^{77}Br[2]	2.4 d	β^+/0.74 EC/99.3	0.36	^{77}Se/7.6 %
^{124}I[3, 4]	4.18 d	β^+/25 EC/75	2.15	^{124}Te/4.8 %
^{86}Y[4, 5]	14.74 hr	β^+/34 EC/66	3.15	^{86}Sr/9.9 %
^{94m}Tc[6]	52 m	β^+/72 EC/28	2.47	^{94}Mo/9.3 %
^{66}Ga[7]	9.49 h	β^+/56,5 EC/43.5	4.15	^{66}Zn/27.8 %
^{60}Cu[8]	23.7 m	β^+/93 EC/7	3.92	^{60}Ni/26.1 %
^{61}Cu[8]	3.33 h	β^+/40 EC/40	1.22	^{61}Ni/1.1 %
^{64}Cu[9]	12.7 hr	β^+/17,4 EC/43 β^-/38	0.66	^{64}Ni/0.9 %
^{45}Ti[10]	3.08 hr	β^+/84,8 EC/15.2	1.04	^{45}Sc/100 %
^{89}Zr[11]	3.27 d	β^+/22,7 EC/77.3	0.90	^{89}Y/100 %
^{52}Mn[12]	5.6 d	β^+/29,6 EC/70.4	0.61	^{52}Cr/84 %

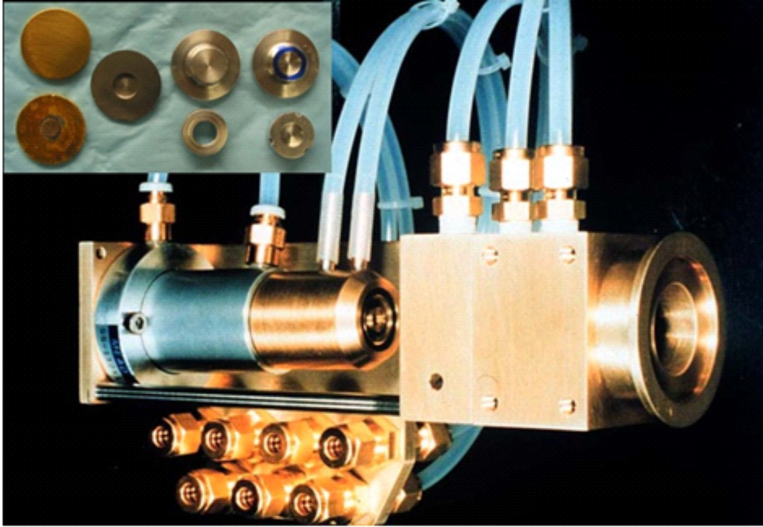TABLE 1. *Characteristics of Nuclides Selected for Production.*

FIGURE 1. *Washington University solid target holder[9]. This target holder is directly attached to the beam and provides for cooling via Helium jet on the front, and via high pressure water flow from the back. Several solid targets are presented on the onset.*

This nuclide is now in production in a weekly basis and we produce for distribution at more than 30 sites in the US. The recuperation of ^{64}Cu proceeds by dissolving the nickel from the gold disk in 6M HCl and then passing the solution through an ion exchange column where both ^{64}Ni and ^{64}Cu can be recuperated[9].

Zr-89 Production

Zr-89 is produced from the (p,n) reaction on natural foil of ^{89}Y and a Niobium target holder. The half-life of 3.27d is particularly well suited for studying the pharmacokinetics of antibodies that can have circulation time of 4-7 days within the body. It is thus a highly sought nuclide for immune-PET imaging which refers to evaluation of patient response to an antibody treatment and also evaluation for individualized patient dosing. The maximum beta energy of 0.9 MeV yield to an average positron range of only 1.2 mm which is not detrimental for PET imaging in clinical setting.

Beta decay proceed to the 9/2+ state of ^{89}Y which has a 16 second half-life. This fortunate situation makes such that this nuclide appears essentially a pure β^+ emitter[11].

Tc-94m Production

The interest of this nuclide is that it could provide an alternative to the highly popular ^{99m}Tc used for SPECT imaging. This nuclide would allow alleviating the limitations of SPECT in terms of sensitivity and resolution. This nuclide is produced via the (p,n) reaction on ^{94}Mo and distillation proceeds through thermal diffusion at 1000 ?C with deposition of the activity on glass tube [6]. The problems with this nuclide are multiples: the maximum positron energy is rather high at 2.47 MeV (low resolution) but also numerous prompt gammas are emitter (high noise). In addition, ^{94g}Tc is co-produced which yield to a more complex decay correction[13]. Indeed, the measured activity being given by the sum of the two states can be represented by:

$$m(t) = A_m(t_{eob})B_m e^{(-\lambda_m t)} + A_g(t_{eob})B_g e^{(-\lambda_g t)} \tag{1}$$

And thus, the 94mTc activity at any given time after end-of-bombardment (*eob*) is given by

$$A_m(t_0) = \frac{m(t)}{B_m e^{(-\lambda_m t)} + (F_g/F_m)B_g e^{(-\lambda_g t)}} \tag{2}$$

Where, $A_m(t)$ and $A_g(t)$ are the activity of the m and g state respectively, and λ_m, λ_g, B_m and B_g are the respective decay constant and beta decay branching ratios. These reasons have contributed to a declining interest in this nuclide. The alternate production strategies for ^{99m}Tc using accelerators or low-enriched uranium (LEU) reactors and improved SPECT camera design are other contributing factor to its demise.

Br-76 and I-124 production

These nuclides are produced by the (p,n) reaction on ^{76}Se or ^{124}Te target[2, 14]. Since Se and Te are brittle, Cu_2Se or Cu_2Te

targets can be used. Alternatively, ^{124}TeO$_2$ have been used. Target distillation proceeds by thermal distillation on a horizontal furnace capable of 1100 C and 1300 C under flow of N$_2$. Activity is transported by the N$_2$ gas and deposited on a Teflon tube. The long half-life of ^{124}I makes production yield very low. Its long half-life makes this nuclide well suited for antibody imaging and since this nuclide is now available commercially, we no longer produce it on a routine basis.

In the next section we will discuss more closely the imaging capabilities of these nuclides in terms of decay characteristics and spatial resolution.

Imaging with Non-standard nuclides

Br-76 deserved some interest due to its decay characteristics. This nuclide decay by beta emission and electron capture to several excited states in ^{76}Se. Notably, decay proceeds at approximately 40 % to excited states at approximately 3 MeV in ^{76}Se. These states will then decay by gamma emission and will result in numerous cascade gamma rays with intense line at 559 keV (74 %). Since the cascade gamma rays are emitted by the daughter nucleus with a very short half-live and the annihilation photons by the emitted positrons, the emission time difference will typically be shorter than the coincidence timing window of the PET scanner and there will be no angular correlation between the cascade gamma ray and the annihilation photons. This will yield to a PET event baring no spatial information on the localization of the activity. Considering that the positron-electron annihilation photons have a fixed energy of 511keV and that typical PET scanner have an energy resolution of 15-20 %, this prompt gamma will be undistinguishable from the annihilation photons and will yield to fortuitous coincidences that will affect image quality, quantitative accuracy and will increase image noise. Others nuclides such as ^{60}Cu, ^{94m}Tc, ^{66}Ga, ^{82}Rb, ^{124}I or ^{86}Y are also notoriously known as "dirty" emitters and call for the application of techniques for correction or elimination for those spurious coincidences.

Cascade Removal Techniques

The most obvious consequence of these fortuitous coincidences from cascade gamma rays is by the appearance of a background of counts in projection space (not image space) which appear at a first approximation as uniform. This observation has thus prompted the implementation of simple uniform background subtraction in the sinograms[15, 16]. Beattie [17, 18] proposed a more elaborate deconvolution technique based on a uniform attenuation inside an ellipse fitted on the patient outline. Based on the observation that the Randoms coincidences have approximately the same distribution as the fortuitous cascade coincidences, it has been proposed that a simple scaling of the randoms distribution can be used. This approach offers very little computational cost and works reliably well for a source of activity not too close to the edge of the field of view. This approach has been implement by Siemens in their scanners. The drawbacks of this technique are that the random distribution is not always available and that this technique do not account for the attenuation of the cascades which may become an issue for large patients.

We proposed an alternative technique for which the cascade coincidence distribution is calculated as a similar fashion as the scatter distribution but for which no angular correlation exists between the cascade gamma ray and the annihilation photon[19]. This technique is based on the fact that the cascade coincidences are not random: they are simply true coincidences with no angular correlation and that their distribution can be exactly calculated knowing the approximate activity distribution and the attenuation image. The drawback is of course the increase computation time.

Indeed, the cascade distribution (in sinogram space) can be calculated by the following volume integral:

$$CC(\rho, \theta, z) = \int_V \frac{A(x, y, z) \exp\left(-\int_{L1} \mu(r) d\vec{r}\right) \exp\left(-\int_{L2} \mu(r) d\vec{r}\right)}{d\Omega_1^2 d\Omega_2^2} dx dy dz$$
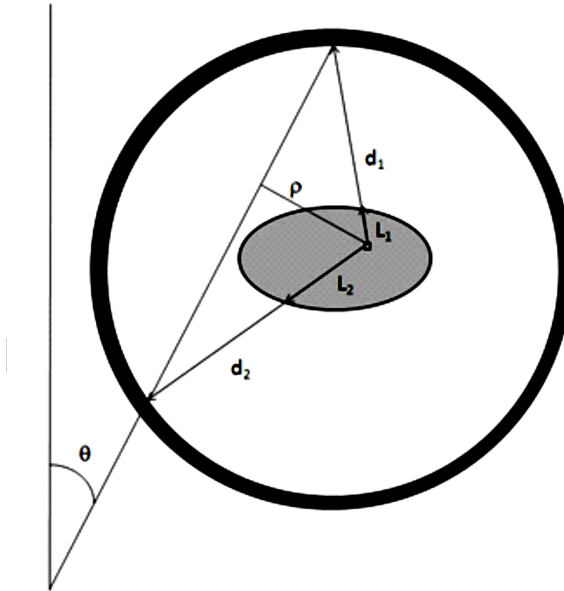
$$(3)$$

FIGURE 2. *Schematic representation of the parameters for cascade distribution calculation. The thick black line represents the PET scanner detector while the shaded ellipse the object being imaged.*

Where $A(x, y, z)$ is the activity concentration at the location x,y,z and $\mu(r)$ is the attenuation coefficient at location $r = \sqrt{x^2 + y^2 + z^2}$, with ρ, θ,z the sinogram projection bin, angle and axial position respectively. This technique allows calculating the functional shape of the distribution, not its magnitude. The distribution can be scaled to the measured sinogram projection profiles by minimizing the function where α and β are scale factors for the Scatter and Cascade distributions.

$$F(\alpha, \beta) = \sum_i [(True_i - \alpha Sc_i - \beta CC_i) \cdot (1 - M_{attn})]^2 \quad (4)$$

The technique result is presented in fig. 3 which shows a projection line profile through a uniform 6 cm diameter [76]Br phantom, taken from [19].
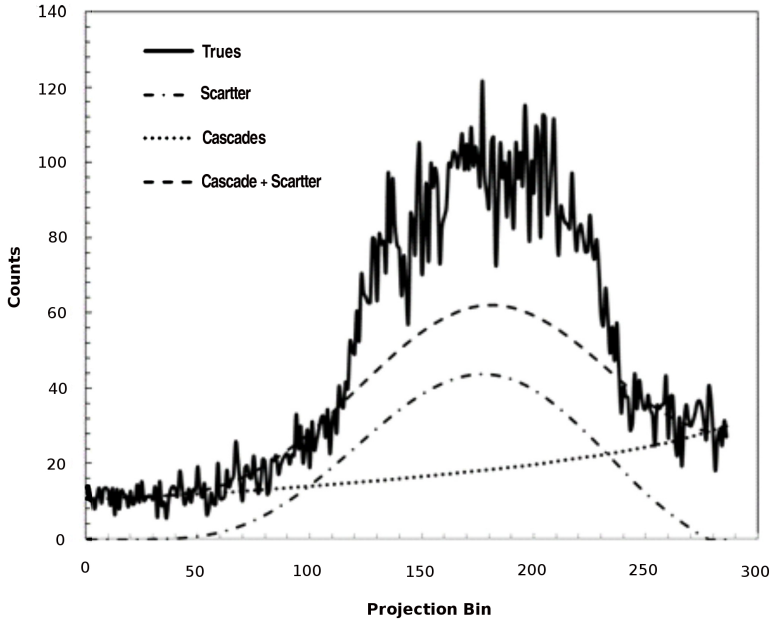
FIGURE 3. *Example of cascade calculated distribution in projection space. The graph shows a profile through the transverse projection data of a phantom filled with Br-76. The dotted line is the result of the cascades calculation while the dot-dashed is the scatter data.*

Image Resolution

Essentially five parameters affect the observed spatial resolution in PET, two of them relates to the fundamental physics of positron decay. These parameters are detector crystal size, crystal penetration and inter-crystal scatter, annihilation photon non-acolinearity, positron range and finally the effects of reconstruction algorithm and the choice of the reconstruction parameters. Most current PET scanners employ the geometry of block detectors arranged in rings perpendicular to the imaging subject. The smallest detection elements is defined by the size of the scintillation crystal within a block and this size defines the sampling distance. Most manufacturers will use interleaving which essentially allows to use a sampling distance at half the crystal-crystal distance. Therefore, the crystal size contribution to

the spatial resolution can be represented by a triangular response
with a width at half the crystal size. The crystal penetration
and inter-crystal scatter refers to the penetration of the gamma
ray through multiple layers of scintillation material and scatter
within a block. This effect is more difficult to calculate but can
be calculated from Monte-Carlo simulations or by the use of an
empirical "block-effect" factor. This factor is particularly spatially
variant and will be responsible for the depth-of-interaction effect
and the loss of resolution outside the central portion of the
field-of-view. The basic physics of positron decay contribution of
photon non-acolinearity can be modelled by a Gaussian distribution
with $\sigma = 0{,}022D$, with D the scanner diameter (in cm). Finally,
the positron range blurring effect is strongly dependent on the
end-point positron energy as well as the specific of the decay
characteristics. Indeed, for nuclides decaying to highly excited
states in the daughter nucleus, the end-point energy will thereby
be reduced and yield to lower positron energy and shorter range
distribution. Finally, the image reconstruction algorithm (and its
parameters) can have a strong influence on the measured spatial
resolution.

The measured spatial resolution is thus be calculated by the
convolution of all these factors as described by [20–22] and results
in a spatially variant spatial resolution that can be characterized
by a single parameter. In [23], we had demonstrated however that
the effective spatial resolution can be more accurately characterized
by the sum of two Gaussian distributions where the first Gaussian
represents the scanner contribution to the resolution and the second
contribution, the contribution from the long positron range for some
nuclides with especially high maximal positron energy.

$$F(x) = \frac{F_1}{\left(\sqrt{2\pi\sigma_1}\right)^3} \exp\left(-\frac{x^2}{2\sigma_1^2}\right) + \frac{1 - F_1}{\left(\sqrt{2\pi\sigma_2}\right)^3} \exp\left(-\frac{x^2}{2\sigma_2^2}\right) \quad (5)$$

Some specially designed image reconstruction algorithms which
include a model of the scanner spatial resolution can in fact improve
the measured spatial resolution and produce optimal image of the
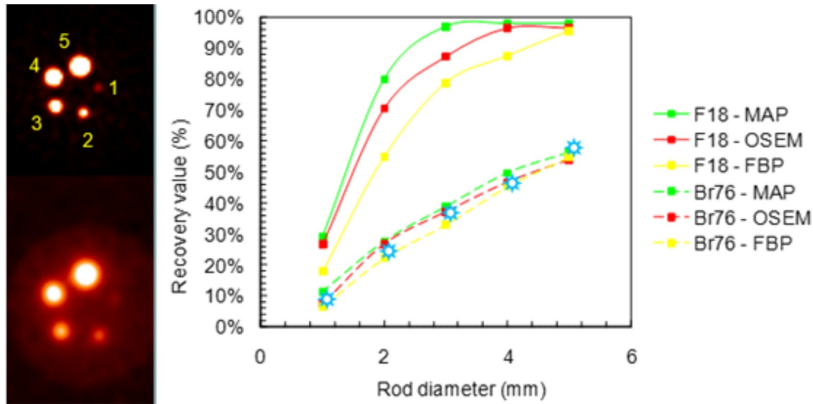activity distribution with both improved resolution and reduced

FIGURE 4. *Example of recovery coefficient measurement for 76Br rod phantom (rods from 1 to 5 mm) and prediction from the double-Gaussian formula above. As a comparison, F-18 recovery coefficients are presented.*

noise. Such algorithms will be topic of the next chapter on PET Image Reconstruction. In this next chapter, we will review the PET technology, principle and image reconstruction theory.

Conclusions

This chapter described the production capabilities of radio-nuclides at Washington University. The production capabilities include all standard PET nuclides and a wide array of non-standard positron emitters that can be used for PET. Equipped with 4 cyclotrons, our center can accommodate our local use in radio-nuclides and the production of some nuclides has a suitable half-life for distribution to any center in North America. We have also discussed the limitations in image quality from the effect of cascade gamma rays and loss of resolution due to the long positron range and proposed correction techniques. In the next chapter, we will expand on this topic by the discussion of resolution recovery image reconstruction algorithm than can account for the positron range.

Acknowledgments

References

[1] T. J. McCarthy, D. W. McCarthy, R. Laforest, H. M. Bigott, F. Wust, D. E. Reichert, M. R. Lewis, and M. J. Welch, AIP Conf. Proc. , 576 (2001), conference date: 1-5 Nov 2000.

[2] V. Tolmachev, A. Lovqvist, L. Einarsson, J. Schultz, and H. Lundqvist, Appl. Radiat. Isot. **49**, 1537 (1998).

[3] D. J. Rowland, R. Laforest, T. J. Mccarthy, B. J. Hughey, and M. J. Welch, J. Labelled Compd. Rad. **44**, S1059 (2001).

[4] J. Schmitz, Eur. J. Nucl. Med. Mol. Imaging , Suppl 1: S4 (2011).

[5] J. Yoo, L. Tang, T. A. Perkins, D. J. Rowland, R. Laforest, J. S. Lewis, and M. J. Welch, Nucl. Med. Biol. **32**, 891 (2005).

[6] H. Bigott, R. Laforest, X. Liu, A. Ruangma, F. Wuest, and M. Welch, Nucl. Med. Biol. **33**, 923 (2006).

[7] M. Lewis, D. E. Reichert, R. Laforest, W. H. Margenau, R. E. Shefer, R. E. Klinkowstein, B. J. Hughey, and M. J. Welch, Nucl. Med. Biol. **29**, 701 (2002).

[8] D. W. McCarthy, L. Bass, P. Cutler, R. Shefer, R. Klinkowstein, P. Herrero, J. Lewis, C. Cutler, C. Anderson, and M. Welch, Nucl. Med. Biol. **26**, 351 (1999).

[9] D. W. McCarthy, R. Shefer, R. Klinkowstein, L. Bass, W. Margeneau, C. Cutler, C. Anderson, and M. Welch, Nuc. Med. Biol. **24**, 35 (1997).

[10] A. L. Vavere, R. Laforest, and M. J. Welch, Nucl. Med. Biol. **32**, 117 (2005).

[11] A. L. Wooten, Appl. Sci. **3**, 593 (2013).

[12] A. L. Wooten, B. Lewis, and S. Lapi, Appl. Radiat. Isot. **96**, 154 (2015).

[13] M. Smith, M. Daube-Witherspoon, P. P.S., L. Szajek,

R. Carson, J. Everett, S. Green, P. Territo, R. Balaban, S. L. Bacharach, and W. Eckelman, Med. Phys. **28**, 36 (2001).

[14] S. M. Qaim, Radiochim **Acta 95**, 67 (2007).

[15] M. Lubberink, H. Schneider, M. Bergstrom, and H. Lundqvist, Phys. Med. Biol. **47**, 3519 (2002).

[16] K. S. Pentlow, R. D. Finn, S. M. Larson, Y. E. Erdi, B. J. Beattie, and J. L. Humm, Clin. Positron Imaging **3**, 85 (2000).

[17] B. J. Beattie, Med. Phys. **30**, 2410 (2003).

[18] B. Beattie and K. Pentlow, J. Nucl. Med. **45(suppl)**, 411P (2004).

[19] R. Laforest and X. Liu, Phys. Med. Biol. **54**, 1503 (2009).

[20] C. S. Levin and E. J. Hoffman, Phys. Med. Biol. **44**, 781 (1999).

[21] C. S. Levin and E. Hoffman, Phys. Med. Biol. **45**, 559 (2000).

[22] R. Laforest, D. Rowland, and M. Welch, IEEE Trans. Nucl. Sci. **49**, 2119 (2002).

[23] X. Liu and R. Laforest, Nucl. Med. Biol. **36**, 551 (2009).